nature communications

Article

https://doi.org/10.1038/s41467-024-54065-9

Approaching the adiabatic infimum of topological pumps on thin-film lithium niobate waveguides

Received: 8 April 2024

Accepted: 31 October 2024

Published online: 12 November 2024

Check for updates

Shengjie Wu[1,2,3], Wange Song[1,2,3] ✉, Jiacheng Sun[1,2,3], Jian Li[1,2,3], Zhiyuan Lin[1,2,3], Xuanyu Liu[1,2,3], Shining Zhu[1,2,3] & Tao Li[1,2,3] ✉

Topological pumps reveal topological insights of adiabatic mode evolution, in which adiabaticity plays a crucial role. However, the adiabatic infimum, i.e., the possible shortest evolution duration of an adiabatic topological pumping process, has remained elusive. In this study, we report the approach of adiabatic infimum in topological pumps in photonic waveguides based on the lithium niobate-on-insulator (LNOI) platform. Besides the most common way to achieve adiabaticity by slowing down the evolution of the system, the adiabaticity of a topological pump is also contingent on an effective Berry connection between instant eigenstates, which can be controlled by the selection of specific pump loops. Specifically, we develop a strategy to identify a pump loop with a minimized effective Berry connection, corresponding to the adiabatic infimum of a topological pump. As such, it is experimentally demonstrated that topological pumps can happen even with rapid evolution speed, at which the conventional pump would completely fail. The adiabatic infimum accelerates the topological pumps from the constraints of slow evolution and facilitates the design of compact topological devices.

Topological photonics, with the emergence of edge states between topologically distinct systems, has opened a promising avenue for robust optical transport and light manipulations[1–4]. Initially proposed by Thouless[5], topological pumps with quantized charge flow in a periodically driven system[6–16] have garnered significant attention and plays a crucial role in realizing robust excitation transfer in finite systems sustaining topological edge states[17–27]. The resilience of topological edge state pumps, protected by the winding of the pump loop around gapless points in parameter space[6–8,12], makes them immune to disorders and defects[12,24]. Topological pump not only provides topological insights into state evolution[21] but also offers a powerful method for exploring higher-dimensional topological physics[14,19]. Importantly, this robust pumping process also holds promise for constituting on-chip functional devices, enabling light manipulations and applications such as quantum state transfer[25–27] and reliable integrated photonic interconnects[24].

A crucial concept underlying these captivating topological pumping phenomena is the adiabaticity[5,6,21,24,28], which necessitates negligible transition between eigenmodes in a time-dependent system and can be characterized by adiabatic criteria[24]. Most previous works fulfill the adiabaticity by simply slowing down parameter modulation[21,23,24], however, the shortest evolution duration required by adiabaticity, termed as the adiabatic infimum, was seldom explored. In fact, the fulfillment of topological pumps only requires the encirclement of the pump loops in the parameter space. The flexible pumping path, which is often overlooked, could provide an opportunity to approach the adiabatic infimum with the fastest topological pumps via exploring the critical loop.

[1]National Laboratory of Solid State Microstructures, College of Engineering and Applied Sciences, Nanjing University, Nanjing, China. [2]Key Laboratory of Intelligent Optical Sensing and Manipulations, Nanjing University, Nanjing, China. [3]Jiangsu Key Laboratory of Artificial Functional Materials, Nanjing University, Nanjing, China. ✉e-mail: songwange@nju.edu.cn; taoli@nju.edu.cn

In this study, we theoretically propose and experimentally demonstrate the adiabatic infimum of topological pumps based on on-chip lithium niobate-on-insulator (LNOI) waveguides. A systematic investigation of the adiabatic criterion reveals the dependence of adiabaticity on the effective Berry connection between different modes and modulation speed. We approach the adiabatic infimum by minimizing the effective Berry connection along the loop, which guarantees fast parameter modulation and realization of the infimum pump at the shortest time/length. Compared to conventional pump schemes, the topological pump can be achieved with half the waveguide length at the adiabatic infimum, showcasing broadband properties according to the adiabatic process and topological nature. Our work addresses the limitation of slow adiabatic evolution in topological pumps via a novel approach that leverages the concept of adiabatic infimum, which opens doors to new possibilities for designing compact topological devices.

Results

Topological pump in the Rice-Mele model

Figure 1a illustrates our idea within a periodically modulated LNOI waveguide lattice based on the Rice-Mele (RM) model[6,7,9,20,21,24]. The RM model comprises staggered on-site potentials and dimerized coupling terms

$$H_{RM}(y) = \sum_{m=1}^{N}(\beta_A(y)|m,A\rangle\langle m,A| + \beta_B(y)|m,B\rangle\langle m,B|) + c_1(y)\sum_{m=1}^{N}(|m,B\rangle\langle m,A| + h.c.) + c_2(y)\sum_{m=1}^{N-1}(|m+1,A\rangle\langle m,B| + h.c.) \quad (1)$$

where y plays the role of time, m denotes the unit cell that comprises two sites (A and B). The on-site energy of the A/B site $\beta_{A,B}(y) = \beta_0 \pm \delta\beta(y)$ and the intracell ($c_1(y) = c_0\text{-}\delta c(y)$) and intercell ($c_2(y) = c_0 + \delta c(y)$) coupling coefficients are subject to periodic modulation with the period P. The periodically modulated RM model inherits the topological nature of the corresponding 2D topological insulator, where the band spectrum under periodic boundary conditions (PBC) can be characterized by Chern number in the momentum-θ (k-θ) space[6,7,9] (see Supplementary Fig. S1).

We consider topological edge pumps in a finite waveguide lattice (unit cell number $N = 4$), which happen when adiabatically varying the parameters (on-site detuning $\delta\beta$ and coupling dimerization δc) to encircle the degeneracy point ($\delta\beta$, δc) = (0,0) in the $\delta\beta$-δc space. Usually, the parameters in a conventional pump scheme are subject to sinusoidal modulation (i.e., $\delta\beta(y) = \delta\beta_0\cdot\sin(2\pi y/P)$ and $\delta c(y) = \delta c_0\cdot\cos(2\pi y/P)$ with $\delta\beta_0$ and δc_0 being the modulation amplitude). Figure 1b shows the eigenvalue spectrum of such lattice during a pump process, where $\theta = 2\pi y/P$ and blue/orange color indicates edge state on left/right boundary and gray indicates bulk modes. Initially ($\theta = 0$), the coupling terms are dimerized ($\delta c > 0$) and the on-site energy of each waveguide is equal ($\delta\beta = 0$). This configuration supports two topological edge states, $|edge_1\rangle$ and $|edge_2\rangle$[29–36], located on the left and right sides of the lattice, respectively. The topological edge states, for example, $|edge_1\rangle$ input from the left ($\theta = 0$) will be pumped to the right side ($\theta = 2\pi$) along the energy level inside the bulk bands (i.e., the pumping channel) after evolving a complete parameter loop.

Such topological pump of edge states necessitates adiabatic conditions described by a criterion[20,21,24]

$$\left|\frac{\left\langle m\left|\frac{d}{dy}\right|edge_1\right\rangle}{\beta_m - \beta_{edge_1}}\right| \ll 1, \quad (2)$$

which characterizes the transition strength between populated eigenstate $|edge_1\rangle$ and all the other instantaneous eigenstates

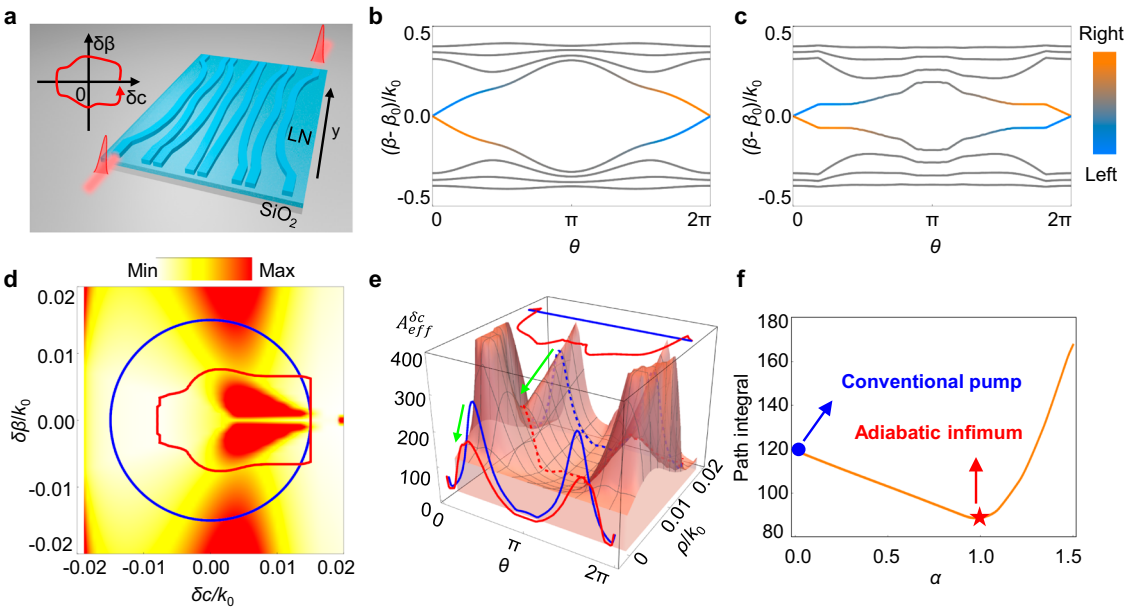

Fig. 1 | Adiabatic infimum of the topological pump and the INFI loop. **a** Illustration of the adiabatic infimum of the topological edge state pump in the LNOI waveguide lattice. **b**, **c** Eigenvalues of RM lattice with $N = 4$ for **b** conventional and **c** INFI the pump schemes. Blue/orange colors indicate left/right edge states, while gray corresponds to bulk modes. **d** $A_{eff}^{\delta c}$ in the $\delta\beta$-δc parameter space. Blue and red trajectories represent the conventional and INFI pump loops, respectively. **e** $A_{eff}^{\delta c}$ and the conventional (blue) and INFI (red) loops in the polar coordinate, where the conventional trajectory climbs some peaks while the INFI loop follows the route in the valleys. The green arrow indicates the decreased direction for better visualization. **f** Integral of $A_{eff}^{\delta c}$ for different loops. The INFI loop (red pentagram) exhibits the minimum integral value, indicating the achievement of adiabatic infimum. $\beta_0 = 1.85k_0$ and $c_0 = 0.02k_0$ with k_0 being the wave vector in vacuum for $\lambda = 1550$ nm.

$|m>(|m>\neq|\text{edge}_1>)$. This criterion can be expanded as

$$\left|\frac{\langle m|\frac{d}{dy}|edge_1\rangle}{\beta_m-\beta_{edge_1}}\right|=\left|\frac{\langle m|\nabla_{\boldsymbol{\gamma}}|edge_1\rangle}{\beta_m-\beta_{edge_1}}\times\frac{d\boldsymbol{\gamma}}{dy}\right|\ll 1,|m\rangle\neq|edge_1\rangle \tag{3}$$

where $\boldsymbol{\gamma}=(\delta\beta,\delta c)$ denotes modulated parameter. Equation (3) provides clear physical insights into the adiabaticity of the considered pump process, which is determined by (1) the effective Berry connection $\mathbf{A}_{eff}(m)$ between $|\text{edge}_1>$ and $|m>$

$$\begin{aligned}\mathbf{A}_{eff}(m)&=\frac{\langle m|\nabla_{\boldsymbol{\gamma}}|edge_1\rangle}{\beta_m-\beta_{edge_1}}=(A_{eff}^{\delta\beta}(m),A_{eff}^{\delta c}(m))\\&=\left(\frac{\langle m|\partial_{\delta\beta}|edge_1\rangle}{\beta_m-\beta_{edge_1}},\frac{\langle m|\partial_{\delta c}|edge_1\rangle}{\beta_m-\beta_{edge_1}}\right)\end{aligned} \tag{3}$$

which describes the transition between two states and depends on the specific parameters $\boldsymbol{\gamma}$, and (2) the modulation speed of parameters $d\boldsymbol{\gamma}/dy$, which usually determines the pumping length. Conventionally, the adiabatic criterion is met by simply decreasing the parameter change speed, thus increases the evolution duration of the system. In what follows, we show that by identifying a pumping loop with minimized effective Berry connection, the topological pump can be accelerated, even approaching the adiabatic infimum with the shortest pumping length.

We first show the $A_{eff}^{\delta c}(m)$ component of effective Berry connection (the $A_{eff}^{\delta\beta}$ component is shown in Supplementary material), and Fig. 1d depicts $A_{eff}^{\delta c}=\max\{A_{eff}^{\delta c}(m)\}$ for $(|m>\neq|\text{edge}_1>)$. The blue circular loop corresponds to the conventional topological pump[9,23,24], which passes through the region with high $A_{eff}^{\delta c}$ values. As a result, the conventional pump scheme requires slow modulation speed along the loop based on Eq. (3). In contrast, if the pump loop can always follow the trajectory with minimized $A_{eff}^{\delta c}$ in the parameter space, the requirement on slow evolution might be relaxed. To address this, we find the parameter loop at the adiabatic infimum (referred as INFI loop) with minimized path integral of the absolute value of $A_{eff}^{\delta c}$, defined as $\min\oint_{\text{loop}}^{\text{pump}}|A_{eff}^{\delta c}|$ (see supplementary material for more detailed discussion), as shown in the red loop in Fig. 1d, which bypasses high effective Berry connection component regions, resulting in a significant drop in $A_{eff}^{\delta c}$ along the INFI loop. The evolution of the energy spectrum along the INFI loop is also depicted in Fig. 1c.

To better illustrate the adiabatic infimum, we analyze the INFI loop under polar coordinate

$$\delta\beta=\rho\cdot\sin(\theta),\delta c=\rho\cdot\cos(\theta) \tag{4}$$

where θ is the argument and ρ is the modulus. Figure 1e shows the $A_{eff}^{\delta c}$ surface as a function of ρ and θ, where the peaks indicate bad adiabaticity. In fact, each topological pumping loop corresponds to a specific function $\rho(\theta)$ with θ ranging from 0 to 2π (for example, the conventional circular loop corresponds $\delta\beta_0=\delta c_0=\rho_{\text{Conv}}$). As shown in Fig. 1e, the conventional and INFI loops are sketched out by dashed blue and dashed red curves on the surface. The exact $A_{eff}^{\delta c}$ value and exact route of each loop with respect to θ is projected to the front and top as the solid blue (conventional)/red (INFI) curves for clear comparison. In contrast to fixing ρ_{Conv} (here $\rho_{\text{Conv}}=0.02k_0$, see projected blue curve on the top) in the conventional loop, which climbs high peaks of $A_{eff}^{\delta c}$ (see projected blue curve on the front), the adiabatic infimum loop is given by searching $\rho_{\text{INFI}}(\theta)$ (see projected red curve on the top) with minimum $A_{eff}^{\delta c}$ for each θ. As a result, the INFI loop goes through the valleys with decreased $A_{eff}^{\delta c}$ in the parameter space (see the projected red curve on the front). To further confirm that the INFI loop indeed corresponds to the adiabatic infimum, we define a parameterized loop $\rho(\theta,\alpha)$, which can continuously deform from the conventional loop ($\rho(\theta,0)$) to the INFI loop ($\rho(\theta,1)$) controlled by the deforming factor α (see Supplementary material for more details). The path integral of $A_{eff}^{\delta c}$ during the parameter winding of different loops (different α) is calculated and shown in Fig. 1f. The loops with $\alpha=0$ (conventional) and $\alpha=1$ (INFI) are marked by blue and red markers, respectively. The integral first decreases as the loop continuously deforms from conventional to INFI loop (α: $0\rightarrow1$) and reaches its minimum at the INFI loop, and then increases with further deformation. The minimum value at the INFI loop clearly verifies the achievement of the adiabatic infimum by INFI method. The $A_{eff}^{\delta\beta}$ component of the effective Berry connection is also analyzed and the INFI loop also can bypass the high $A_{eff}^{\delta\beta}$ region (see Supplementary material).

Illustration of fast topological pumps at the adiabatic infimum

To quantitatively explore the infimum of the adiabatic condition, we define the fidelity as $|<\Psi(y)|\text{edge}_1(y)>|^2$, where $|\Psi(y)>$ represents the optical field at y. Figure 2a, b illustrate the fidelity throughout the pump process for the conventional and INFI loops, respectively, which are calculated based on the coupled mode theory (CMT)[28–30]. The white dashed lines correspond to the fidelity along the pumping process for periods increasing from 100 μm to 1000 μm in steps of 100 μm. The output fidelity with respect to different pump period is highlighted as the solid blue/red line for the conventional/INFI loop. As the period increases, the topological pump process can be divided into three regions: nonadiabatic regions-I and -II, and adiabatic region-III. In region-I, the output fidelity rises with increasing period. The short period leads to nonadiabatic evolution due to fast parameter changes, causing fidelity oscillations during the evolution. At the crossing point of region-I and -II, the light predominantly exits from the last waveguide, which is the result via direct coupling between neighboring waveguides rather than the effect of adiabatic topological pumps. The significant fidelity oscillation along the decrease (white dashed line at $L=200$ μm) suggests that the transitions between different eigenstates during light propagation occur in a manner that violates the adiabatic condition. The direct coupling-induced phenomenon is fundamentally sensitive to parameter variations. Therefore, increasing the period in region-II violates critical parameters, resulting in decreased output fidelity. In adiabatic region-III, the fidelity during the pumping process remains near 1, indicating that the light field is pinned to the eigenstate $|\text{edge}_1>$ during adiabatic evolution. Consequently, the unitary output fidelity is maintained even further increasing the pump period. The crossing point of region-II and -III indicates the shortest length required for the adiabaticity of the corresponding pump loop, which is $L_{\text{Conv}}=700$ μm for the conventional loop (Fig. 2a) and shortened to $L_{\text{INFI}}=400$ μm for the INFI loop (Fig. 2b).

The output intensity calculated using CMT for different periods is depicted in Fig. 2c, where the red (blue) line corresponds to the INFI (conventional) structure. When the waveguide length falls within regions-I and -II (e.g., 100 μm), adiabaticity cannot be fulfilled for both designed lattices, resulting in the spread of the output signal along the lattice. Upon increasing the period to the critical adiabatic length (e.g., $L_{\text{INFI}}=400$ μm and $L_{\text{Conv}}=700$ μm, indicated by the orange and blue arrows, respectively), the output signal emerges from the right edge of the lattice. Further increasing the waveguide length in region-III does not significantly affect the output. The CMT-calculated field evolutions at L_{INFI} and L_{Conv} are shown in Fig. 2d, where the left (right) panel in each box corresponds to the conventional (INFI) lattice. For the conventional lattice, the adiabaticity cannot be met at $L=L_{\text{INFI}}$, and the light spreads into the bulk at the output (Fig. 2d, left panel in orange box). In contrast, the adiabatic condition is fulfilled for the INFI lattice at this short length, which is attributed to the decreased sensitivity along the INFI loop. As a result, the light field follows the eigenstate evolution of $|\text{edge}_1>$ and comes out from the right edge (Fig. 2d, right panel in orange box). At the long waveguide length $L=L_{\text{Conv}}$, both the INFI and the conventional lattices fall in the adiabatic

https://doi.org/10.1038/s41467-024-54065-9

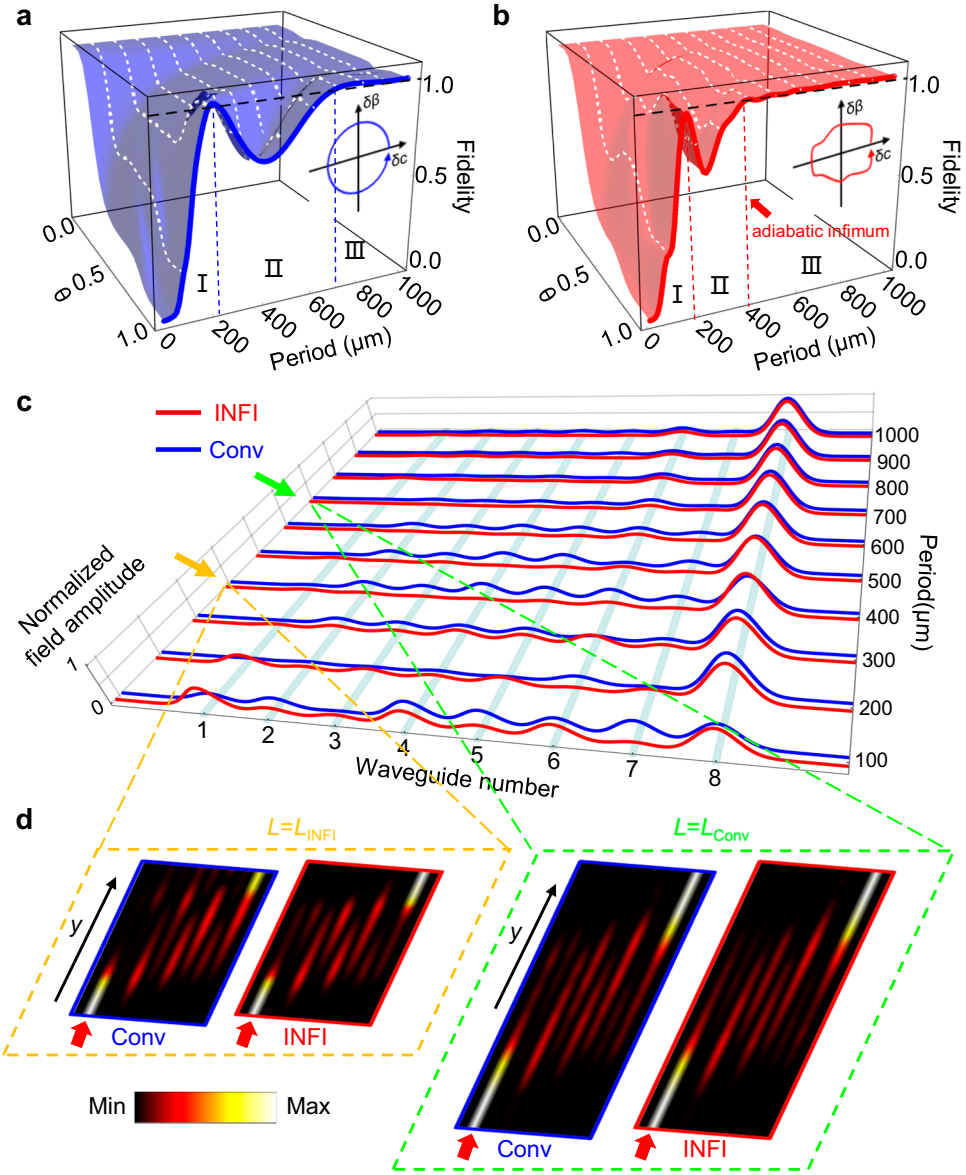

Fig. 2 | Optical field evolution in the INFI and conventional waveguide lattices. **a**, **b** Field fidelity along the pump process for (**a**) conventional and (**b**) INFI designs with respect to different pump periods. Output fidelities are highlighted with blue and red lines, respectively. **c** The CMT calculated output signals with varying lattice lengths for the conventional (blue) and INFI (red) structures. **d** CMT-calculated field evolution at $L = L_{INFI}$ (orange box) and $L = L_{Conv}$ (green box). At $L = L_{INFI}$, the input signal is pumped to the right edge in the INFI lattice (right panel), while it spreads along the lattice in the conventional lattice (left panel). At $L = L_{Conv}$, the signal mainly emerges from the 8th waveguide in both lattices.

region, and the output signals locate on the edge waveguide (Fig. 2d, green box).

Experimental results

In experiments, we fabricate four types of samples on the X-cut LNOI platform, i.e., lattice under conventional pump scheme with two different lengths $L = L_{Conv}$ and $L = L_{INFI}$, and lattice under INFI pump scheme also with two different lengths $L = L_{Conv}$ and $L = L_{INFI}$. A grating coupler is connected to the first waveguide in the RM lattice through an adiabatic taper to couple the light into the edge state of the waveguide lattice. Coupling-out gratings (labeled as O1 ~ O8 in Fig. 3a) are connected to each waveguide at the output facet. The light propagates along the y-axis of X-cut LN material with refractive index $n_e = 2.21$ for transverse electric (TE) modes at 1550 nm. The LNOI waveguide consists of a 300 nm thick film (h_2) and 300 nm ridge (h_1) (see Supplementary material for details). The waveguide lattices are designed by mapping $\beta_{A,B}(y)$, and $c_{1,2}(y)$ to the waveguide width $w_{A,B}$, and gap between adjacent intra/inter-cell waveguides (see Supplementary Material for details). The samples are fabricated using the method of electron beam lithography (EBL) and the dry etching process (see Method for details). Figure 3a displays the optical propagations captured by CCD in experiments for INFI sample at $L = L_{INFI}$, the light comes out from the opposite side of the sample, indicating the fulfillment of the topological pumps. The enlargement of the output signal is shown in the right panel of Fig. 3c, with the simulated light evolution displayed in the bottom. The simulated field evolution clearly shows that the edge state is adiabatically pumped to the other side of the waveguide lattice, which is fully consistent with the experiment. In contrast, the light field evolves nonadiabatically in the conventional lattice at $L = L_{INFI}$, and the output signal spreads into the bulk (left panel in Fig. 3c). At $L = L_{Conv}$, the adiabatic condition is met for both lattices, and the input light evolves along $|edge_1\rangle$ and

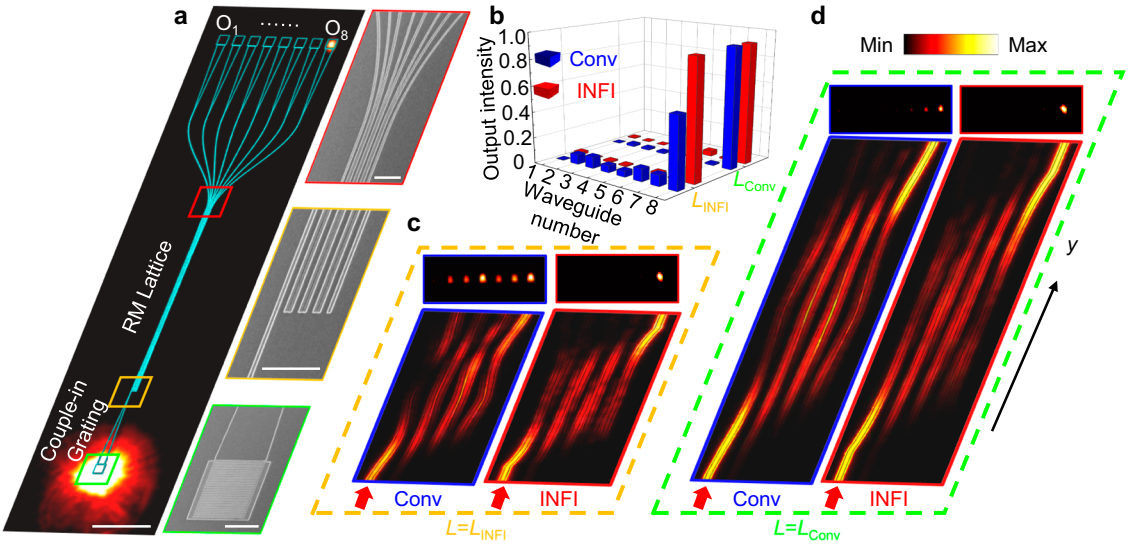

Fig. 3 | Experimental demonstration. a Optical microscope photograph (left) and enlarged SEM pictures (right) of the sample. The scalar bars in the optical microscope image and SEM pictures correspond to 100 μm and 10 μm, respectively. **b** Numerically simulated output signal for the INFI and conventional lattices at $L = L_{INFI}$ and $L = L_{Conv}$. Experimental captured output signal (top) and simulated field evolution (bottom) for corresponding structures, with blue/red frames indicating conventional/INFI structures at (**c**) $L = L_{INFI}$ and (**d**) $L = L_{Conv}$.

comes out from the right edge of the lattice (see Fig. 3d). The numerically simulated output intensities for the INFI and conventional pumps are presented in Fig. 3b, clearly demonstrating that the INFI design indeed can fulfill the topological pumps at a shorter length compared to the conventional case (see Supplementary Material for details). Furthermore, the INFI lattice at $L = L_{INFI}$ exhibits broadband edge state pump (from 1500 nm to 1650 nm) while the conventional lattice at $L = L_{INFI}$ fails to pump the edge states within the entire bandwidth (see Supplementary Material for more details).

Discussion

In summary, we have demonstrated the adiabatic infimum of the topological pump in a periodically driven Rice-Mele model on the LNOI waveguide. To be mentioned, the implementation of fast evolution in the LNOI platform holds particular importance, because the LN waveguides have a lower refractive index compared with Si ones, which usually prevents the compact integration in the LNOI chip. Our investigation into the effective Berry connection of instant eigenstates within the parameter space leads to its minimization along the adiabatic infimum pump loop, which features the shortest evolution length while preserving the adiabaticity. Consequently, a fast topological pump is achieved, which transfers broadband light with a much shorter device length compared to the conventional pump scheme. Our investigation into the adiabatic infimum provides deep insights into the understanding of adiabaticity of topological evolutions and the demonstrated fast topological pump on the LNOI platform greatly favors compact topological photonic applications.

Methods

Sample fabrication

The experimental samples were fabricated using the method of electron beam lithography (EBL) and the dry etching process. The substrate used here is a 500-μm Si substrate with 600-nm Lithium Niobate deposition. The substrates were cleaned in an ultrasound bath in acetone, isopropyl alcohol (IPA), and DI water for 15 min respectively, and dried under clean nitrogen flow. The waveguide arrays and grating nanostructures were exposed to EBL. The samples were then used to dry etch the Lithium Niobate layer in a 16:1 mixture of Ar and CHF_3 plasma and the residual photoresist was stripped off by an oxygen plasma stripper.

Optical measurement

A telecom-band laser (Fianium-1550-SF) with tunable laser frequency was used to characterize the fabricated sample. The laser beam with its polarization being controlled by a polarizer was focused on the grating coupler A(B) from the substrate side by the Mitutoyo near-infrared (NIR) long-working distance object OF (100×, Numerical Aperture (NA) = 0.70, focal length (f) = 200 mm). The transmitted signal was coupled into free space from the air side via the grating coupler B(A) in the forward (backward) case. The output signal was collected by a NIR imaging object OI (50×, NA = 0.42, f = 200 mm) and imaged on a near-infrared charge-coupled device (CCD) camera (Xenics Xeva-1.7-320).

Data availability

The data that support the findings of this study are provided in the Supplementary Information/Source Data file. Source data are provided with this paper.

References

1. Wang, Z., Chong, Y., Joannopoulos, J. D. & Soljačić, M. Observation of unidirectional backscattering-immune topological electromagnetic states. *Nature* **461**, 772–775 (2009).
2. Hasan, M. Z. & Kane, C. L. Colloquium: topological insulators. *Rev. Mod. Phys.* **82**, 3045–3067 (2010).
3. Qi, X.-L. & Zhang, S.-C. Topological insulators and superconductors. *Rev. Mod. Phys.* **83**, 1057–1110 (2011).
4. Bansil, A., Lin, H. & Das, T. Colloquium: topological band theory. *Rev. Mod. Phys.* **88**, 021004 (2016).
5. Thouless, D. J. Quantization of particle transport. *Phys. Rev. B.* **27**, 6083 (1983).
6. Citro, R. & Aidelsburger, M. Thouless pumping and topology. *Nat. Rev. Phys.* **5**, 87–101 (2023).
7. Lohse, M., Schweizer, C., Zilberberg, O., Aidels-burger, M. & Bloch, I. A. Thouless quantum pump with ultracold bosonic atoms in an optical superlattice. *Nat. Phys.* **12**, 350–354 (2016).
8. Ke, Y. et al. Topological phase transitions and Thouless pumping of light in photonic waveguide arrays. *Laser Photon. Rev.* **10**, 995–1001 (2016).
9. Nakajima, S. et al. Topological Thouless pumping of ultracold fermions. *Nat. Phys.* **12**, 296–300 (2016).

10. Wang, P. et al. Two-dimensional Thouless pumping of light in photonic moiré lattices. *Nat. Commun.* **13**, 6738 (2022).
11. Fu, Q., Wang, P., Kartashov, Y. V., Konotop, V. V. & Ye, F. Nonlinear Thouless pumping: solitons and transport breakdown. *Phys. Rev. Lett.* **128**, 154101 (2022).
12. Cerjan, A., Wang, M., Huang, S., Chen, K. P. & Rechtsman, M. Thouless pumping in disordered photonic systems. *Light. Sci. Appl.* **9**, 178 (2020).
13. Xu, Z., Zhang, Y. & Chen, S. Topological phase transition and charge pumping in a one-dimensional periodically driven optical lattice. *Phys. Rev. A* **96,** 013606 (2017).
14. Lohse, M., Schweizer, C., Price, H. M., Zilberberg, O. & Bloch, I. Exploring 4D quantum Hall physics with a 2D topological charge pump. *Nature* **553**, 55–58 (2018).
15. Fedorova, Z., Qiu, H., Linden, S. & Kroha, J. Observation of topological transport quantization by dissipation in fast Thouless pumps. *Nat. Commun.* **11**, 3758 (2020).
16. Silva, S. V., Fernandes, D. E., Morgado, T. A. & Silveirinha, M. G. Topological pumping and Tamm states in photonic systems. *Phys. Rev. B* **105**, 155133 (2022).
17. Kraus, Y. E., Lahini, Y., Ringel, Z., Verbin, M. & Zilberberg, O. Topological states and adiabatic pumping in quasicrystals. *Phys. Rev. Lett.* **109**, 106402 (2012).
18. Verbin, M., Zilberberg, O., Lahini, Y., Kraus, Y. E. & Silberberg, Y. Topological pumping over a photonic Fibonacci quasicrystal. *Phys. Rev. B* **91**, 064201 (2015).
19. Zilberberg, O. et al. Photonic topological boundary pumping as a probe of 4D quantum Hall physics. *Nature* **553**, 59–62 (2018).
20. Longhi, S. Topological pumping of edge states via adiabatic passage. *Phys. Rev. B* **99**, 155150 (2019).
21. Chen, Z., Tang, W., Zhang, R., Chen, Z. & Ma, G. Landau-Zener transition in the dynamic transfer of acoustic topological states. *Phys. Rev. Lett.* **126**, 054301 (2021).
22. Benalcazar, W. A. et al. Higher-order topological pumping and its observation in photonic lattices. *Phys. Rev. B* **105**, 195129 (2022).
23. Cheng, Q. et al. Asymmetric topological pumping in nonparaxial photonics. *Nat. Commun.* **13**, 249 (2022).
24. Sun, L. et al. Broadband and fabrication tolerant power coupling and mode-order conversion using Thouless pumping mechanism. *Laser Photon. Rev.* **16**, 2200354 (2022).
25. Palaiodimopoulos, N. E., Brouzos, I., Diakonos, F. K. & Theocharis, G. Fast and robust quantum state transfer via a topological chain. *Phys. Rev. A* **103**, 052409 (2021).
26. Longhi, S., Giorgi, G. L. & Zambrini, R. Landau-Zener topological quantum state transfer. *Adv. Quantum Tech.* **2**, 1800090 (2019).
27. Mei, F., Chen, G., Tian, L., Zhu, S. & Jia, S. Robust quantum state transfer via topological edge states in superconducting qubit chains. *Phys. Rev. A* **98**, 012331 (2018).
28. Wu, S. et al. Broadband asymmetric light transport in compact lithium niobate waveguides *Laser Photon. Rev* **17**, 2300306 (2023).
29. Song, W. et al. Breakup and recovery of topological zero modes in finite non-Hermitian optical lattices. *Phys. Rev. Lett.* **123**, 165701 (2019).
30. Song, W. et al. Robust and broadband optical coupling by topological waveguide arrays. *Laser Photon. Rev.* **14**, 1900193 (2020).
31. Cheng, Q., Pan, Y., Wang, Q., Tao, L. & Zhu, S. Topologically protected interface mode in plasmonic waveguide arrays. *Laser Photon. Rev.* **9**, 392 (2015).
32. Wang, Y. et al. Coherent interactions in one-dimensional topological photonic systems and their applications in all-optical logic operation. *Nano Lett.* **20**, 8796–8802 (2021).
33. Poli, C., Bellec, M., Kuhl, U., Mortessagne, F. & Schomerus, H. Selective enhancement of topologically induced interface states in a dielectric resonator chain. *Nat. Commun.* **6**, 6710 (2015).
34. Zhao, H. et al. Topological hybrid silicon microlasers. *Nat. Commun.* **9**, 981 (2018).
35. Kruk, S. et al. Nonlinear light generation in topological nanostructures. *Nat. Nanotechnol.* **14**, 126–130 (2019).
36. Redondo, A. et al. Topological optical waveguiding in silicon and the transition between topological and trivial defect states. *Phys. Rev. Lett.* **116**, 163901 (2016).

Acknowledgements

The authors acknowledge the financial support from The National Key R&D Program of China (2022YFA1404301(T. L.), 2023YFA1407700(W. S.)), National Natural Science Foundation of China (No. 12174186(T. L.), No. 12204233(W. S.), No. 62325504(T. L.), No. 62288101(T. L.), No. 92250304(T. L.)). Tao Li thanks to the support from the Dengfeng Project B of Nanjing University.

Author contributions

T. L., S. W., and W. S. developed the idea. S. W. and W. S. proposed the design. S. W. performed the theoretical calculation and numerical simulation. J. S. and J. L. fabricated the samples. S. W. and W. S. performed the optical measurement with assistance from Z. L. and X. L. T. L. supervised the project. S. W., W. S., S. Z., and T. L. analyzed the results. S. W., W. S., and T. L. wrote the manuscript. All authors contributed to discussions.

Competing interests

The authors declare no competing interests.

Additional information

Supplementary information The online version contains supplementary material available at https://doi.org/10.1038/s41467-024-54065-9.

Correspondence and requests for materials should be addressed to Wange Song or Tao Li.

Peer review information *Nature Communications* thanks Chiara Devescovi, and the other, anonymous, reviewer(s) for their contribution to the peer review of this work. A peer review file is available.